Available online at www.jourcc.com

Journal homepage: www.JOURCC.com

Journal of Composites and Compounds

Effect of austenitic stainless steel cladding on the high-temperature oxidation resistance of ferritic 2.25Cr-1Mo (Grade 22) steel using the SMAW process

Hassan Jafarikhorami [a]*

[a] *Department of Materials, Science and Research Branch, Islamic Azad University (IAU), Tehran, Iran*

A B S T R A C T

The high-temperature oxidation resistance of low alloy steel affected by the cladding of austenitic stainless steel has been investigated in this study. For this purpose, Shielded Metal Arc Welding (SMAW) technique was used to prepare a proper layer of AISI347 on the surface of ferritic steels. The microstructure and morphology properties of the alloys were examined using transmission electron microscopy (TEM), scanning electron microscopy (SEM), and Energy Dispersive X-Ray Analysis (EDX) techniques. Results demonstrated that the construction of oxide shells on the surface of non-modified ferritic steel was responsible for its low resistance in contrast to the oxidation at high-temperature conditions. The oxidation screening of coated and uncoated samples with tuning time at constant temperature showed the increased oxidizing intensity of both materials. Conversely, with tuning temperature from 850 to 950 oC at a constant time, an abnormal increase was observed in oxidation intensity. The corresponding k_ps of the uncoated sample was determinate 1.27708×10^{-8}, 3.267×10^{-8}, and the corresponding k_ps of coated material was determinate 54.5×10^{-10}, 6.6×10^{-10}. The performed investigation proved that the formation of oxidized compact needle microstructures in the resulting alloy is the reason for the extraordinarily oxidizing resistance of austenitic stainless steel.

Peer review under responsibility of JCC Research Group

A R T I C L E I N F O R M A T I O N

Article history:
Received 17 April 2021
Received in revised form 03 June 2021
Accepted 25 June 2021

Keywords:
Ferritic steels
Cr-Mo steel
SMAW technique
austenitic steel
Corrosion resistance
Oxidation

1. Introduction

The alloy of 2.25Cr-1Mo (ASTM Grade 22) is low-alloy ferritic-bainitic steel. This was developed for high-temperature applications and is also being applied primarily in the current systems of energy generation [1], properly considered as an alternative material for pressure containers of nuclear power plants (NPPs) at high-temperature conditions [2-4]. The radiation resistance [5, 6], high-temperature creep [7], welding [8, 9], and the microstructure [8] of 2.25Cr–1Mo steel have been widely investigated during the last three decades. Additionally, some researchers are keen on the wearing and corrosion of this material and have performed several explorations [10, 11]. Recently, Wang et al. have studied the tangential fretting wear of 2.25Cr–1Mo steel and the effect of 2.25Cr–1Mo steel wear behavior at high temperatures [10, 12].

Having enough stability, mechanical properties, and ease of fabrication are additional requirements. Stability, requires corrosion and oxidation resistance, microstructural stability, and resistance to graphitization that is a requisite for creep resistance. The thermal efficiency in power generation relies on operating temperatures, thus there has been, and remains, a constant striving to find material technologies that enable higher operating temperatures. This is the case in applications such as turbine materials and the operating temperatures of heat exchangers and pipes. In a typical application, Grade 22 steel is applied for superheater tubing and filler metal for joining steam piping because of its good creep-rupture strength [13, 14] and radiation resistance [15-17] as mentioned above.

Bainitic alloys have been developed to prepare analogous creep properties, with excellent weldability, but they will be more susceptible to oxidation. Since the 1990s, the focus of the development of power plant steels has been on higher chromium alloys that provide increased oxidation resistance, while minimally reduces its ductility [18].

The steam generated by boilers passes through the superheater tubes to produce superheated steam. The superheater tubes are frequently subjected to failures due to corrosion-related issues. The materials of superheater tubes are selected for a specific design life in a complex situation involving high temperature, pressure, and corrosive environment. The 2.25Cr-1.0Mo low-alloy steel is one of the most common materials used for the construction of super heater tubes due to its high-temperature mechanical strength and great corrosion resistance. However, as a result of improper operation conditions such as temperature runaway or inadequate corrosion mitigation, superheater tubes are susceptible to failure mechanisms such as oxygen pitting [19, 20], creep [21, 22], thermal fatigue [22, 23], temper embrittlement [24], and stress corrosion cracking (SCC) [25, 26]. Stress corrosion cracking occurs when tensile

* *Corresponding author: Hassan Jafarikhorami; Email: jafarikhorami@gmail.com*
DOR: 20.1001.1.26765837.2021.3.7.3.8
https://doi.org/10.52547/jcc.3.2.3

Fig. 1. The images of a plate; (a) primary plate (before creption), (b) plate after creption, and (c) polished creptsample.

stress, corrosive environment, and susceptible material exist at the same time. In boilers built with carbon and low-alloy steel tubes, oxygen and sodium hydroxide are corrosive agents that can cause SCC failures [27]. Research works have indicated that induced pits due to poor water treatment may act as stress concentrators for the initiation of the cracks [28].

In welded tubes, a strength mismatch between weld deposit and base metal due to great hardenability of 2.25Cr-1.0Mo steel increases cracking occurrence in the tube weldment [28]. Therefore, post-weld heat treatment of weld in 2.25Cr-1.0Mo tubes, in addition to reducing residual stress, is necessary to minimize strength and hardness mismatch by the reduction of weldment hardness [29].

Furthermore, studies have demonstrated that the use of more corrosion-resistant materials, including stainless steel, effectively limits the boiler equipment corrosion, helping the lifetime duration of boilers. However, this is expensive, and interesting aims are to provide a cost-effective substitute to the application of cheaper materials, such as Fe-2.25Cr-1Mo (as low-alloy steel) and high-temperature operations. To make this possible while maintaining a reasonable lifetime of the boiler equipment, it is necessary to understand the underlying mechanisms of the rapid corrosion of low-alloy steels necessitating a better understanding of the effect of existing corrosive species. There are a few essays that closely investigate the influence of some elements such as chlorine-containing composites, particularly alkali chlorides [30], on high-temperature corrosion of low-alloy steels [31], pure iron [32], and stainless steels [33].

In addition, while it is well-known that oxygen-released compounds cause oxidation and corrosion in all these materials, the underlying mechanisms of this element are still under discussion. Herein, we aim to study the effect of austenitic stainless steel cladding on the high-temperature oxidation resistance of ferritic 2.25Cr-1Mo (Grade 22) steel, which has not been studied so far. For this purpose, the SMAW technique was applied to prepare a suitable layer of AISI347 over the surface of ferritic steels. The microstructure and morphology properties were examined in the resulted alloys.

2. Materials and methods

2.1. Materials

The material used in this study is 20 plates of ASTM A387 Grade 22 steel (Table 1), prepared with equal dimensions (40×30×10 mm). Austenitic steel (E347-16) purchased from Methrod Co. (the UK) was employed as the coating metal SMAW was used to clad austenitic steel over each Fe-Cr-Mo plate.

2.2. Sample preparation

Table 1.
Chemical composition of the consumed steel as a substrate

%Mo	%Cr	%Si	%S	%P	%Mn	%C
0.99	2.32	0.45	0.03	0.028	0.4	0.13

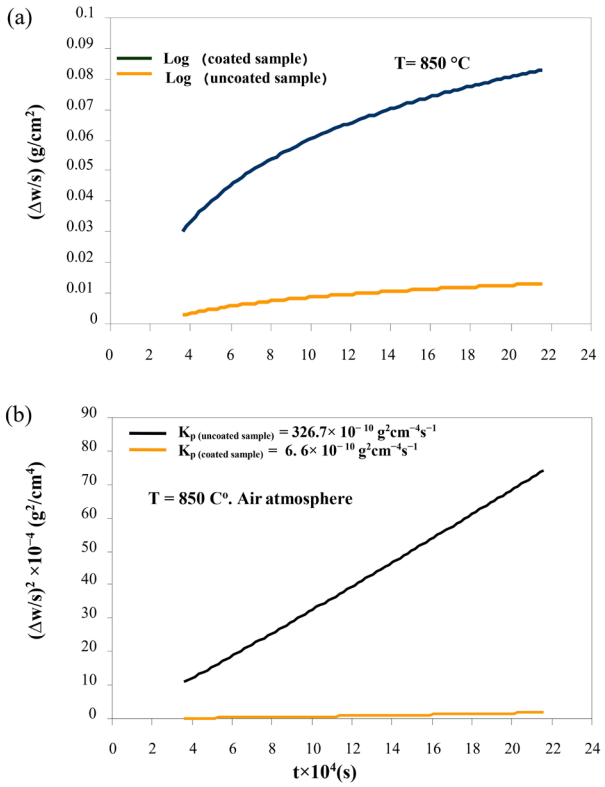

Fig. 2. Air oxidation weight gains of the uncoated and coated samples oxidized at 850 °C; (a) weight gain against time and (b) squared weight gain against time.

The crept specimens were sectioned on the upper surface of 10 samples, to comparison 10 others plates without crepitation. Note that none of the samples had obvious necking regions and the samples were extracted in such a way to examine the surface parallel to the loading axis, as shown schematically in Figure 1.

The extracted samples were polished in multiple stages using a diamond paste (3-μm solution, followed by 1-μm solution) and colloidal silica (15-nm solution) before the hardness measurements.

2.3. Characterization

To investigate and identify the type and number of induced oxide phases on the surface of the samples in the oxidation test, the XRD analysis was used using the PAN Analytical instrument (Model X'Pert PROMPD, the Netherlands). The growth of oxide layers depends on the ability of oxygen to penetrate and the morphology of the primary oxide shells. The morphology of the detected shells on the oxidation effect was studied by a SEM (JEOL model JSM-6610LV, Japan) equipped with EDS of Oxford instrument facility (model number 51-ADD0013).

3. Results and discussions

3.1. Oxidation kinetics

The weight gain of the samples per unit area (Δw/s) versus time (t) is shown in Figure 2a. This exhibits the results of tThermogravimetric analyses of steels containing 2.25 Cr-1Mo (AISI A387) as the substrate steel (uncoated) and austenitic stainless steel AISI 347 as the coated steel coated at 850 °C inside the furnace for 60 h.

For the comparison of weight increase of uncoated and coated samples (Fig 2a), the weight gain of coated samples was almost uniform and low, contrary to the uncoated samples. On the other hand, uncoated samples have a significant weight increase due to the high rate of oxidation. Fig 2b shows the ratio of $(\Delta w/s)^2$ to the times for coated and uncoated

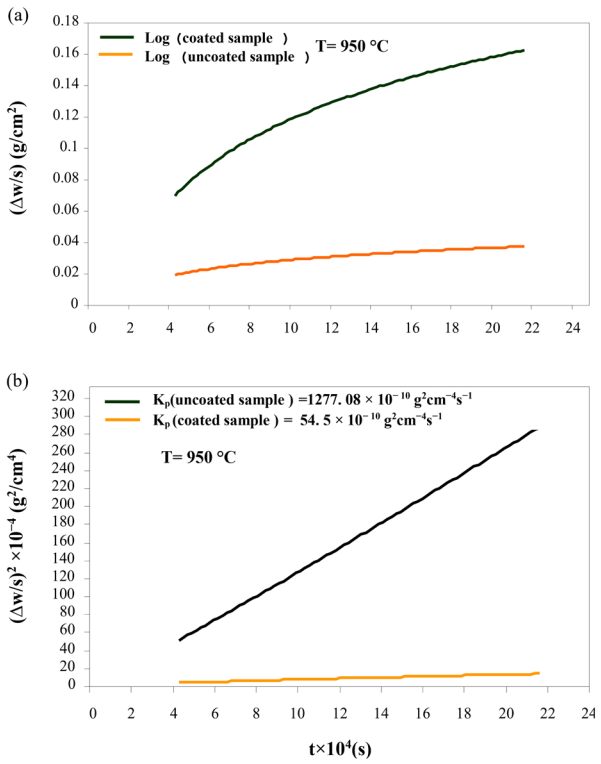

Fig. 3. Air oxidation weight gains of the uncoated and coated samples oxidized at 950 °C; (a) weight gain against time and (b) squared weight gain against time.

samples at 850 °C.

In most cases, there is a linear relationship between the ratio $(\Delta w/s)^2$ and (t), which indicates the parabolic law corresponding to Eq. 1"

$$(\Delta w / s)^2 = K_p . t \quad (1)$$

where "w" is the weight gain of the samples, "s" is the area, and "t" is time. The parabolic relationship indicates that the growth of oxide shells is a function of diffusion, and "K_p" as a coefficient for the growth rate of Cr oxide is proportional to the penetration of oxygen. The "K_p" coefficients for coated and uncoated samples at the tested temperatures are given in Table 2.

By comparing Figure 2a and 3a, it seems that increasing the temperature from 850 °C to 950 °C has little effect on the growth rate of the oxides and the increase in weights of the uncoated and the coated samples relative to each other. However Fig 3a depicts a large difference between the weight increase of coated and uncoated samples. Fig 3b also shows a ratio of $(\Delta w/s)^2$ for coated and uncoated samples at 950 °C. Although in the thermogravimetric analysis of samples at two applied temperatures, the effect of temperature is not very considerable, in comparison to Figures 2b and 3b, there is a remarkable difference in the ratio of $(\Delta w/s)^2$. This means that the growth rate of oxide layers in uncoated samples at 950 °C is much higher than that at 850 °C, but the growth rate does not change considerably in coated samples.

Fig. 4 shows a comparison of a ratio of $(\Delta w/s)^2$ for coated samples at both 850 and 950 °C. At 850 °C the ratio of $(\Delta w/s)^2$ increased linearly, while it was almost curved at 950 °C, and did not change markedly in comparison with the uncoated samples. Persdotter et al [30] investigated

Table 2.
K_p coefficients at the tested temperatures

Temperature (°C)	AISI347	2.25Cr-1Mo
850	6.6 ×10−10	3.267 × 10−8
950	54.5×10−10	1.27708 × 10−8

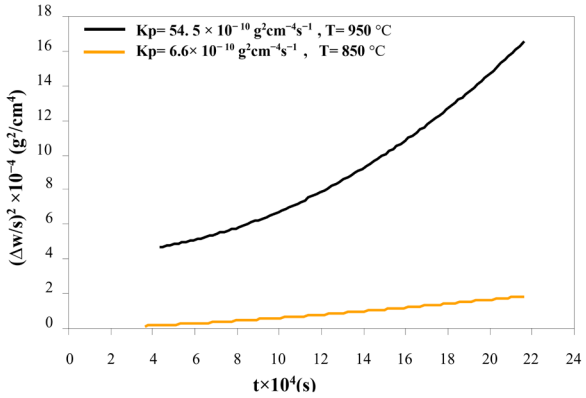

Fig. 4. Comparison of squared weight gain of samples per unit time for coated samples at 850 and 950 °C.

the oxidation of Fe-2.25Cr-1Mo in presence of KCl(s) at 400 °C and crack formation and its influence on oxidation kinetics. Their results show slow parabolic kinetics recorded by TGA, which indicates that the oxide growth is diffusion-controlled in good agreement with previous studies [31, 34, 35]. The difference in parabolic rate constant between iron and Fe-2.25Cr-1Mo observed in their study indicates that the presence of chromium, detected in the inward growing spinel, has an important influence on the overall growth rate at 400 °C.

3.2. Surface morphology examination

SEM images with a magnification of 15000x were also used to compare the morphology of the oxides. As mentioned in the previous sections, the test variables were time and temperature. To study the morphology of surface oxides for both uncoated and coated samples, the times of 10 h and 60 h were selected at both temperatures of 850 and 950 °C.

Figure 5 (a and b) shows the SEM images of the uncoated sample, which was placed in a normal atmosphere furnace at 850 °C for 10 h and 60 h. As expected, there are iron-rich phases on the oxidized surface of the uncoated sample. The types of these phases will be specified by XRD analysis in the next section.

Figur 5a clearly defines the block-shaped surface oxides. Open spaces between oxide blocks are the best place for oxygen to penetrate the substrates and this will increase the oxidation rate in uncoated samples. This will cause the oxide shells formed during servicing of these steels at high temperatures to easily accelerate oxidation from the separated surface. Moreover, peeling off the oxide blocks will reduce the thickness of the relevant sheet and thus reduce the service time of the part.

Figure 5b also shows the SEM image of the uncoated sample kept in the furnace at 850 °C at a maximum time of 60 h. At a constant temperature, increasing the oxidation time will certainly lead to the growth of oxidative shells which is understood by examining and observing Figure 5 (a and b). The growth of oxide blocks was oberved with increasing time from 10 h to 60 h, and their compaction decreased compared to 10 h. Figure 5 (a and b) is presented to investigate the effect of time on the morphology of surface oxides.

To study the effect of temperature, it was necessary to take pictures of samples that were oxidized at 950°C in proportion to 10 and 60 h.

Figure 5c shows the SEM image of a sample placed in a furnace at 950 °C for 10 h. Comparing Figure 5 a and c, the effect of temperature is well visible. Increasing the temperature will increase the growth rate of oxide layers and shells. On the other hand, comparing Fig 5a and c reveals that the growth rate of oxide layers is almost the same. Increasing both the temperature and the oxidation time will lead to a decrease in the height of block-shaped oxides, which will sometimes increase the adhesion of the oxide shells. Jagadeeswara Rao et al. [36] studied at-

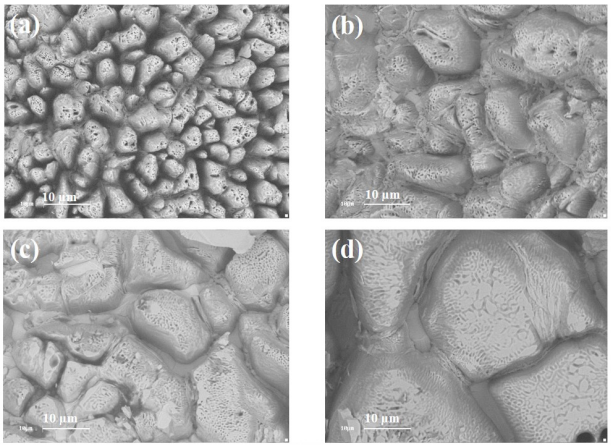

Fig. 5. SEM image of uncoated sample, oxidized in (a) T = 850 °C, t = 10 h (15000x), (b) T = 850 °C, t = 60 h (15000x), (c) T = 950 °C, t = 10 h (15000x), and (d) T = 950 °C t = 60 h (15000x).

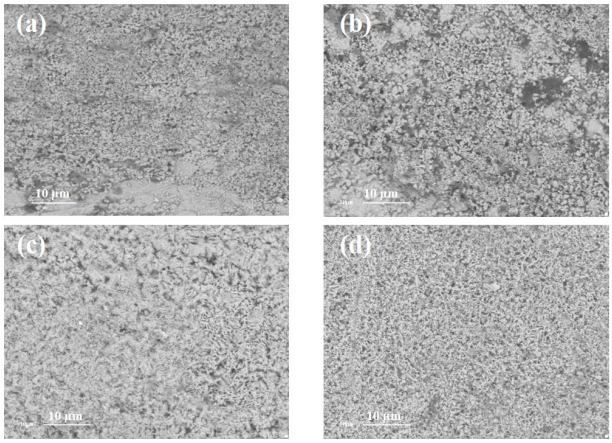

Fig. 6. SEM image of the coated sample, oxidized in (a) T = 850 °C, t = 10 h (15000x), (b) T = 850 °C, t = 60 h (15000x), (c) T = 950 °C, t = 10 h (15000x), and (d) T = 950 °C, t = 60 h (15000x).

mospheric air oxidation of 9Cr-1Mo steel and found that as increasing the time of oxidation to 50 h increased the size of the oxide globules, yielding two different morphologies of platelet and globules.

Unlike uncoated samples whose surface morphology was in the form of block-shaped oxides, the morphology of the oxides in coated samples is needle-shaped and compact in structure. Figure 6 (a and b) show the SEM images of the coated samples, which were placed in an oven at 850 °C for 10 h and 60 h. As can be seen from Fig 6a, the needle-shaped oxides are observed in coated samples. The compactness of these needle-shaped oxide layers is considered to be the most important reason for increasing oxidation resistance because it has made it difficult for oxygen to penetrate the underlying layers and this has reduced the oxidation rate in coated samples. Similarly, to investigate the effect of oxidation time on coated samples, a comparison was made between SEM images at longer times. Figure 6b shows the SEM image of the coated sample, kept in an oven at 850 °C for 60 h. Comparing Fig 5a and b, it seems that increasing the oxidation time did not have much effect on the surface morphology of the samples at a constant temperature. The only effect that will increase over time is a slight increase in the weight of the samples due to oxidation. Figure 6 (c and d) shows the SEM images of a sample placed in a furnace at 950 °C for 10 h and 60 h to investigate the effect of increasing the temperature from 850 °C to 950 °C on the morphology of surface oxides.

Increasing the temperature led to an increase in the number of oxide needles per unit area. In other words, due to the formation of compressed oxide needles, the weight gain rate of coated samples significantly declined compared to uncoated samples in the same conditions and compared to a sample placed in the furnace at 850 °C for 10 h. The needles did not grow but became more compact. On the other hand, increasing the time from 10 to 60 h at 950 °C will make the oxide needles more compact, which will create a stronger barrier against oxygen penetration and thus reduce the oxidation rate at high temperatures.

According to the result of the EDX analysis, the peaks indicate iron-rich oxide phases, with the difference that the intensity of these peaks is relatively higher than previous peaks, which confirms the increase in the percentage of oxide phases. EDX analysis also shows the presence of Cr-rich phases along with iron-rich phases. In the next section, the types of phases formed on the surface of coated samples will be fully discussed based on XRD analysis. Unlike uncoated samples, EDX analysis in coated samples did not differ much between the obtained peaks. This means that the thickness of the needle-shaped layers was not very large, but the increase in time and temperature caused the compression of the oxide layers.

3.3. Phase analysis

As shown in the previous section and according to the relevant SEM images, only the growth of the initial phases was observed that occurred in the first stage of the experiment, i.e. at 10 h and 850 °C. For this reason, the samples were subjected to an XRD test by applying both the maximum temperature and oxidation test time. Among the uncoated samples, a sample was selected that was exposed to a temperature of 950 °C for 60 h. Figure 7a shows the XRD analysis image of the uncoated sample, which along with the obtained results, can prove with certainty that the iron-rich phases will include the oxidative phases of Fe_2O_3, Fe_3O_4, and FeO. Also, some Fe-Cr-O compound in the form of $FeCr_2O_4$ is present in the formed oxide shells due to the presence of Cr in the substrate steel. In contrast, the XRD analysis was performed to investigate the type and number of phases formed on the surface of coated samples from a sample that was in the oven at 950 °C for 60 h. Fig 7b shows the XRD analysis image of this sample.

As shown in Figure 7b, the phases that formed in the coated samples were Cr_2O_3, Fe_2O_3, and some of the oxide phases of CrO_2. CrO_2 oxide will usually form at temperatures above 1100 °C, which will reduce the oxidation resistance due to the porosity of the oxide-shaped needle shells. Creating any porosity will increase the possibility of oxygen penetration and thus increase the rate of oxidation. In this sample, some of

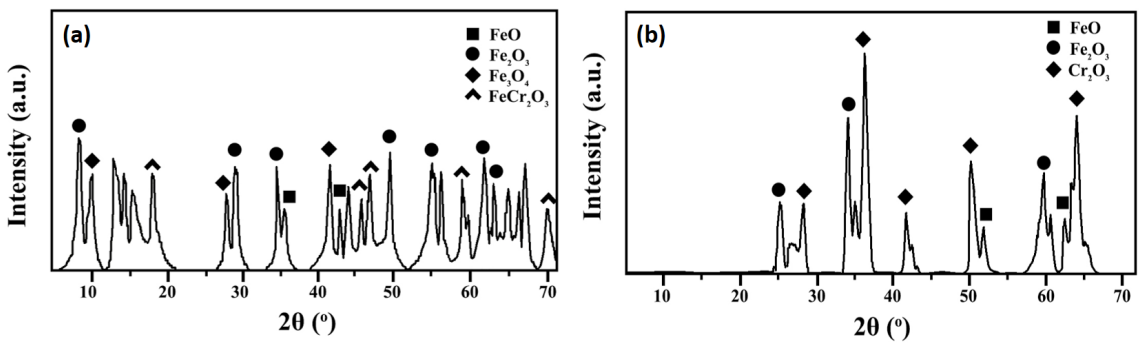

Fig. 7. XRD analysis images of (a) uncoated and (b) coated samples oxidized at T = 950 °C, t = 60 h.

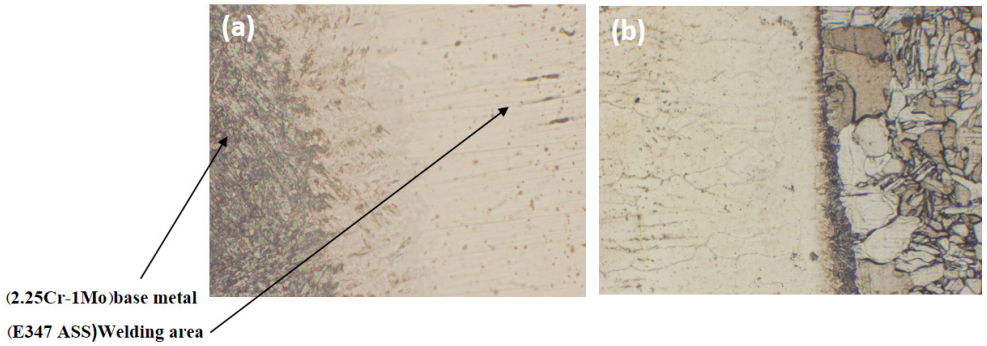

Fig. 8. Metallographic images of (a) the weld affected area and (b) the area affected by welding after the oxidation test at T= 850 °C, t = 10 h (x200).

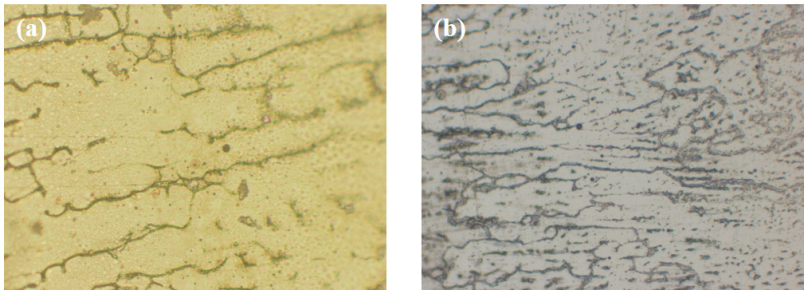

Fig. 9. Metallographic images of (a) the welding area and (b) the weld zone after oxidation at T = 850 °C, t = 10 h (x200).

this free phase was formed due to storage at 950 °C for a long time (60 h), but it had little effect on reducing oxidation resistance due to a low temperature in this experiment. Earlier studies show that the oxidation of ferritic steels can result in the formation of a multi-layered oxide scale on the surface consisting of Fe_2O_3, Fe_3O_4, and FeO [37, 38].

3.4. Microstructural degradation of weldments

To study the microstructure of the weldments, it was necessary to first prepare the cross-section of the samples and then sand and polish them. For this purpose, sanding numbers of 120, 240, 280, 360, 400, 600, 800, and 1000 were used, respectively, for pre-prepared sections. Then, images of the coated samples were taken with a light microscope before and after the oxidation test.

In this section, an attempt is made to provide a brief and useful explanation of the effects of oxidation time and temperature on the area affected by welding and the welding area, along with the relevant metallographic images. Figure 8a shows a metallographic image of the weld affected area at 200x magnification before any oxidation test. As a result of welding in an area as narrow as 60 µm, it has changed and is out of coaxial state.

Figure 8b shows a metallographic image of a welding-affected area after an oxidation test at 850 °C for 10 h. As can be seen in Figure 8 (a and b), storage at 850 °C will reduce the size of the area affected by welding. On the other hand, the base metal grains have returned to their original state, i.e. coaxial grains due to the infiltration phenomenon.

Figure 9a shows a metallographic image of the weld zone before the oxidation test and after welding. Unlike the affected area, the oxidation test had little effect on the weld area. Since the weld metal contains between 5 and 10% ferrite, storage at this temperature and time has only resulted in partial cohesion of the ferrite veins, which have grown somewhat during the oxidation test. Figure 9b shows a metallographic image of a boiling point exposed to 850 °C for 10 h.

The effect of time was investigated on the area affected by welding and the welding area. Figure 9b shows the metallographic images of the weld area oxidized at 850 °C for 10-60 h. According to Figure 10 (a and b), increasing the oxidation time at a constant temperature will not have a significant effect on the microstructure of the weld area. Figure 10 (c and b) also shows the metallographic image of the weld zone subjected to oxidation at 850 °C for 10 and 60 h. In this case, the increase in time did not affect the welding area.

The effect of temperature was investigated on the area affected by welding and the boiling area.

The effect of temperature increase will be much greater than time. Figure 11 shows a metallographic image of a weld-affected area that was subjected to oxidation at 850 and 950 °C for 60 h. Comparing Figure 11a and b will conclude that increasing the temperature from 850 to 950 °C leads to the growth of central coaxial grains and the base metal, and the area and width of the affected area are reduced by boiling. Figure 11 (c and d) shows the metallography of the weld zone, which was subjected to oxidation at 850 and 950 °C for 60 h. Unlike the area affected by welding and the base metal, the increase in temperature did not have much effect on the metallographic structure of the weld area.

Table 3.
Chemical composition of the uncoated and coated samples obtained from the EDS analysis

Sample	O	Fe	Cr	Mo
Uncoated oxidized sample at T = 850°C, t = 10h	63.74	25.50	6.36	4.40
coated oxidized sample at T = 850°C, t = 10h	58	27	8.70	6.30

4. Conclusions

Forming a protective layer of cream on the surface of stainless steel will have a significant effect on protection against corrosion and oxidation at high temperatures. Suitable for various applications, stainless steels are widely used, especially in pipelines, pressure vessels, and heat exchangers, whose application temperature can reach up to 1100 °C. Due to the lower cost and the lower thermal expansion coefficient of ferritic steels, such as one containing 2.25Cr-1Mo, than austenitic stainless steels, these steels will be a suitable alternative. Because of the need to apply higher temperatures, on the other hand, the use of austenitic stainless steel coating seems a logical method due to the formation of a protective layer of Cr. In this study, the effect of 347 austenitic stainless steel coating was investigated on the oxidation behavior of steel contain-

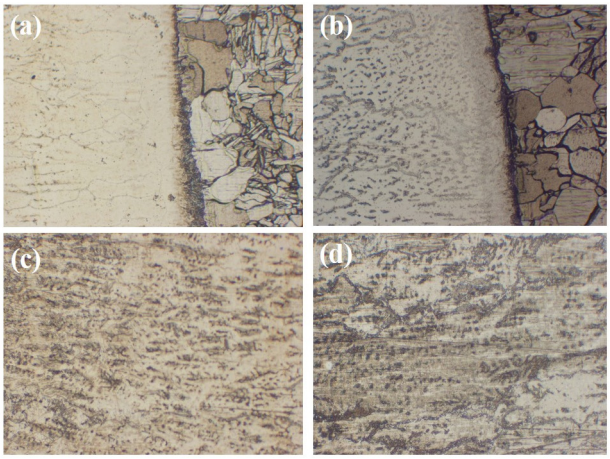

Fig. 10. The metallographic image of the weld affected area lasted (a) 10 h and (b) 60 h at 850 °C (x200), and metallographic image of the welding area during (c) 10 h and (d) 60 h at 850 °C (x200).

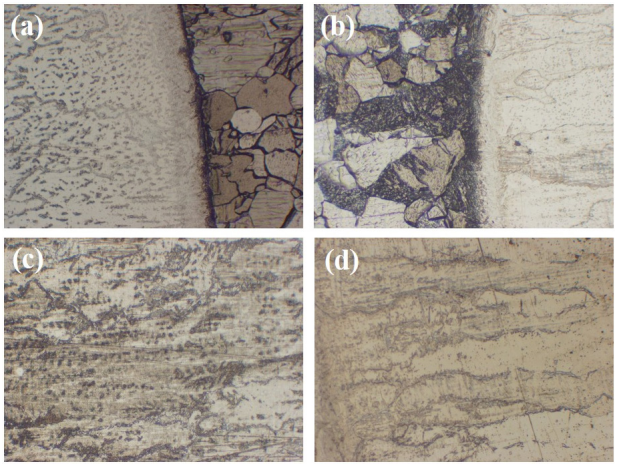

Fig. 11. Metallographic image of the affected area for 60 h at (a) 850 °C and (b) 950 °C (x200) and metallographic image of the welding area for (a) 60 h at 850 °C and (b) 950 °C (x200).

ing 2.25Cr-1Mo at a high temperature, along with analyzing the mechanism of formation of protective oxide layers. The findings showed that the stainless steel coating reduced the intensity of oxidation, especially at 950 °C. Examination of the morphology of oxide layers shows the structure of coaxial oxide shells in uncoated samples and compressed oxide needles in coated samples. At both temperatures, the oxidation intensity increased with increasing time at a constant temperature, while an abnormal increase in oxidation intensity was observed at a constant time with increasing the temperature from 850 to 950 °C. Uncoated samples at 850 and 950 °C had oxidation constants of (Kp) of 3.267×10^{-8} and 1.27708×10^{-8}, respectively, and those for coated samples were 6.6×10^{-10} and 54.5×10^{-10} at 850 and 950 °C, respectively. Studies have shown that the oxidation resistance of austenitic stainless steel is due to the formation of oxidized compact needles.

Acknowledgments

The authors would like to acknowledge Islamic Azad University (IAU) for the financial support towards this research.

Conflict of interest

The authors declare that there is no conflict of interest.

REFERENCES

[1] F. Masuyama, Advances in creep damage/life assessment technology for creep strength enhanced ferritic steels, Procedia Engineering 55 (2013) 591-598.
[2] O. Muránsky, H. Zhu, S.-L. Lim, K. Short, J. Cairney, M. Drew, On the evolution of mechanical properties and microstructure of ferritic-bainitic (FB) 2.25 Cr-1Mo (Grade 22) steel during high-temperature creep, Materialia 9 (2020) 100513.
[3] S.J. Zinkle, Advanced irradiation-resistant materials for Generation IV nuclear reactors, Structural Materials for Generation IV Nuclear Reactors, Woodhead Publishing, Buckingham, England, UK, 2017, pp. 569-594.
[4] D. Blagoeva, L. Debarberis, M. Jong, P. Ten Pierick, Stability of ferritic steel to higher doses: Survey of reactor pressure vessel steel data and comparison with candidate materials for future nuclear systems, International Journal of Pressure Vessels and Piping 122 (2014) 1-5.
[5] J. Calaf Chica, P.M. Bravo Díez, M. Preciado Calzada, A new prediction method for the ultimate tensile strength of steel alloys with small punch test, Materials 11(9) (2018) 1491.
[6] J. Bulloch, A study concerning material fracture toughness and some small punch test data for low alloy steels, Engineering Failure Analysis 11(4) (2004) 635-653.
[7] M.T. Whittaker, B. Wilshire, Advanced procedures for long-term creep data prediction for 2.25 chromium steels, Metallurgical and Materials Transactions A 44(1) (2013) 136-153.
[8] S. Ren, S. Li, Y. Wang, D. Deng, N. Ma, Finite element analysis of residual stress in 2.25 Cr-1Mo steel pipe during welding and heat treatment process, Journal of Manufacturing Processes 47 (2019) 110-118.
[9] A. Elrefaey, Y. Javadi, J.A. Francis, M.D. Callaghan, A.J. Leonard, Evolution of microstructure and toughness in 2.25 Cr-1Mo steel welds, International Journal of Pressure Vessels and Piping 165 (2018) 20-28.
[10] X.-d. Chen, L.-w. Wang, L.-y. Yang, R. Tang, Y.-q. Yu, Z.-b. Cai, Investigation on the impact wear behavior of 2.25 Cr–1Mo steel at elevated temperature, Wear 476(2021) 203740.
[11] R. Sahoo, B. Jha, T. Sahoo, S. Mantry, Effect of microstructural degradation on solid particle erosion behavior of 2.25 Cr-1Mo steel, Tribology Transactions 57(4) (2014) 679-689.
[12] X.-D. Chen, L.-W. Wang, L.-Y. Yang, R. Tang, Z.-B. Cai, Effects of Temperature on the Fretting Wear Behavior of 2.25 Cr-1Mo Tubes against Gr_5C_{12} Rods, Materials 13(15) (2020) 3388.
[13] M. Whittaker, B. Wilshire, Long term creep life prediction for Grade 22 (2· 25Cr—1Mo) steels, Materials Science and Technology 27(3) (2011) 642-647.
[14] K. Maruyama, K. Sawada, J. Koike, H. Sato, K. Yagi, Examination of deformation mechanism maps in 2.25 Cr—1Mo steel by creep tests at strain rates of 10^{-11} to 10^{-6} s^{-1}, Materials Science and Engineering: A 224(1-2) (1997) 166-172.
[15] R. Klueh, A.T. Nelson, Ferritic/martensitic steels for next-generation reactors, Journal of Nuclear Materials 371(1-3) (2007) 37-52.
[16] H. Bhadeshia, A. Strang, D. Gooch, Ferritic power plant steels: remanent life assessment and approach to equilibrium, International materials reviews 43(2) (1998) 45-69.
[17] S.C. Deevi, Advanced Intermetallic Iron Aluminide Coatings for High Temperature Applications, Progress in Materials Science 118(2020)100769.
[18] S. Dépinoy, C. Toffolon-Masclet, S. Urvoy, J. Roubaud, B. Marini, F. Roch, E. Kozeschnik, A.-F. Gourgues-Lorenzon, Carbide precipitation in 2.25 Cr-1 Mo bainitic steel: effect of heating and isothermal tempering conditions, Metallurgical and Materials Transactions A 48(5) (2017) 2164-2178.
[19] K. Ranjbar, Failure analysis of boiler cold and hot reheater tubes, Engineering Failure Analysis 14(4) (2007) 620-625.
[20] A. Heyes, Oxygen pitting failure of a bagasse boiler tube, Engineering Failure Analysis 8(2) (2001) 123-131.
[21] A. Saha, H. Roy, Failure investigation of a secondary super heater tube in a 140 MW thermal power plant, Case Studies in Engineering Failure Fnalysis 8 (2017) 57-60.
[22] A. Alvino, D. Lega, F. Giacobbe, V. Mazzocchi, A. Rinaldi, Damage characterization in two reformer heater tubes after nearly 10 years of service at different operative and maintenance conditions, Engineering Failure Analysis 17(7-8) (2010) 1526-1541.
[23] A. Usman, A.N. Khan, Failure analysis of heat exchanger tubes, Engineering Failure Analysis 15(1-2) (2008) 118-128.
[24] Z. PENG, W. REN, C. YANG, F. CHEN, H. LIU, F. PENG, Q. MEI, Relationship between the evolution of phase parameters of grain boundary $M_{23}C_6$ and embrittlement of HR_3C super-heater tubes in service, Acta Metall Sin 51(11) (2015) 1325-1332.
[25] C.A. Duarte, E. Espejo, J.C. Martinez, Failure analysis of the wall tubes of a water-tube boiler, Engineering Failure Analysis 79 (2017) 704-713.
[26] S. Xu, C. Wang, W. Wang, Failure analysis of stress corrosion cracking in heat exchanger tubes during start-up operation, Engineering Failure Analysis 51

(2015) 1-8.
[27] J.J. Aumuller, V.A. Carucci, Determination of Service Life for Undamaged and Damaged Delayed Coker Drums, ASME 2016 Pressure Vessels and Piping Conference, American Society of Mechanical Engineers Digital Collection 50398(2016) V003T03A059.
[28] A. Ahmadi, M. shayegani Akmal, A. Pasha, S. Yareie, Failure analysis of cracked 2.25 Cr–1.0 Mo steel tubes of an oil refinery boiler, Engineering Failure Analysis 110 (2020) 104435.
[29] M. Nakano, T. Tanaka, M. Abe, M. Nakatani, H. Terasaki, Improvement of Low-Temperature Toughness in Weld Metal Made of 9Cr-1Mo-V Steel by GTAW Method, Pressure Vessels and Piping Conference, American Society of Mechanical Engineers 58981(2019) V06BT06A005.
[30] A. Persdotter, M. Sattari, E. Larsson, M.O. Ogaz, J. Liske, T. Jonsson, Oxidation of Fe-2.25 Cr-1Mo in presence of KCl (s) at 400° C–Crack formation and its influence on oxidation kinetics, Corrosion Science 163 (2020) 108234.
[31] M.A. Olivas-Ogaz, J. Eklund, A. Persdotter, M. Sattari, J. Liske, J.-E. Svensson, T. Jonsson, The Influence of Oxide-Scale Microstructure on KCl (s)-Induced Corrosion of Low-Alloyed Steel at 400 C, Oxidation of Metals 91(3) (2019) 291-310.
[32] H. Ma, C. Zhou, L. Wang, High temperature corrosion of pure Fe, Cr and Fe–Cr binary alloys in O_2 containing trace KCl vapour at 750° C, Corrosion Science 51(8) (2009) 1861-1867.
[33] J. Sui, J. Lehmusto, M. Bergelin, M. Hupa, The effects of KCl, NaCl and K_2CO_3 on the high-temperature oxidation onset of sanicro 28 steel, Oxidation of metals 85(5-6) (2016) 565-598.
[34] N. Folkeson, T. Jonsson, M. Halvarsson, L.G. Johansson, J.E. Svensson, The influence of small amounts of KCl (s) on the high temperature corrosion of a Fe-2.25 Cr-1Mo steel at 400 and 500° C, Materials and Corrosion 62(7) (2011) 606-615.
[35] T. Jonsson, N. Folkeson, J.-E. Svensson, L.-G. Johansson, M. Halvarsson, An ESEM in situ investigation of initial stages of the KCl induced high temperature corrosion of a Fe–2.25 Cr–1Mo steel at 400 C, Corrosion Science 53(6) (2011) 2233-2246.
[36] C.J. Rao, S. Ningshen, J. Philip, Atmospheric air oxidation of 9Cr-1Mo steel: Depth profiling of oxide layers using glow discharge optical emission spectrometry, Spectrochimica Acta Part B: Atomic Spectroscopy 172 (2020) 105973.
[37] S.B. Ranganath, C.D. Wick, B.R. Ramachandran, Role of Structure and Oxidation States in the Passivation of Stainless Steel by Chromium, group 29 (2019) 33.
[38] M. Weiser, R.J. Chater, B.A. Shollock, S. Virtanen, Transport mechanisms during the high-temperature oxidation of ternary γ/γ′ Co-base model alloys, NPJ Materials Degradation 3(1) (2019) 1-11.